THE JOURNAL OF BIOLOGICAL CHEMISTRY VOL. 283, NO. 24, pp. 16830–16839, June 13, 2008

Crystal Structure of Human Liver Δ^4-3-Ketosteroid 5β-Reductase (AKR1D1) and Implications for Substrate Binding and Catalysis*[S]◆

Received for publication, March 5, 2008, and in revised form, April 9, 2008 Published, JBC Papers in Press, April 11, 2008, DOI 10.1074/jbc.M801778200

Luigi Di Costanzo[‡], Jason E. Drury[§], Trevor M. Penning[§1], and David W. Christianson[‡2]

From the [‡]Roy and Diana Vagelos Laboratories, Department of Chemistry, University of Pennsylvania, Philadelphia, Pennsylvania 19104-6323 and the [§]Center of Excellence in Environmental Toxicology and the Department of Pharmacology, University of Pennsylvania School of Medicine, Philadelphia, Pennsylvania 19104-6084

AKR1D1 (steroid 5β-reductase) reduces all Δ^4-3-ketosteroids to form 5β-dihydrosteroids, a first step in the clearance of steroid hormones and an essential step in the synthesis of all bile acids. The reduction of the carbon–carbon double bond in an α,β-unsaturated ketone by 5β-reductase is a unique reaction in steroid enzymology because hydride transfer from NADPH to the β-face of a Δ^4-3-ketosteroid yields a *cis*-A/B-ring configuration with an ~90° bend in steroid structure. Here, we report the first x-ray crystal structure of a mammalian steroid hormone carbon–carbon double bond reductase, human Δ^4-3-ketosteroid 5β-reductase (AKR1D1), and its complexes with intact substrates. We have determined the structures of AKR1D1 complexes with $NADP^+$ at 1.79- and 1.35-Å resolution (HEPES bound in the active site), $NADP^+$ and cortisone at 1.90-Å resolution, $NADP^+$ and progesterone at 2.03-Å resolution, and $NADP^+$ and testosterone at 1.62-Å resolution. Complexes with cortisone and progesterone reveal productive substrate binding orientations based on the proximity of each steroid carbon–carbon double bond to the *re*-face of the nicotinamide ring of $NADP^+$. This orientation would permit 4-pro-(*R*)-hydride transfer from NADPH. Each steroid carbonyl accepts hydrogen bonds from catalytic residues Tyr^{58} and Glu^{120}. The Y58F and E120A mutants are devoid of activity, supporting a role for this dyad in the catalytic mechanism. Intriguingly, testosterone binds nonproductively, thereby rationalizing the substrate inhibition observed with this particular steroid. The locations of disease-linked mutations thought to be responsible for bile acid deficiency are also revealed.

The Δ^4-3-ketosteroid functionality is present in all steroid hormones except estrogens. The first step in their metabolism involves the reduction of the Δ^4-ene to produce either 5α- or 5β-dihydrosteroids in reactions catalyzed by steroid 5α- or 5β-reductase, respectively (1). These two enzymes belong to distinct gene superfamilies (2, 3), and structural information on these enzymes is currently lacking.

Δ^4-3-Ketosteroid 5β-reductase is a soluble monomeric NADPH-dependent enzyme and a member of the aldo-keto reductase (AKR)[3] superfamily and is designated AKR1D1 in humans (3, 4). In utilizing NADPH as hydride donor, the enzymatic reaction introduces a 90° bend at the steroid A/B-ring junction, which adopts a *cis*-A/B- or β-configuration (Fig. 1) (5–7). In the absence of enzyme catalysis, this reaction is extremely difficult to perform with chemical reductants. Treatment with borohydride favors formation of the 3β-allylic alcohol, and under harsher conditions, the 3β,5α-tetrahydrosteroid is formed (8, 9). It is possible to generate a 5β-cholestane from the corresponding Δ^4-3-ketosteroid only if a large directing group is placed at C-4 or C-7 to direct the face of hydride addition or catalytic hydrogenation (10, 11). Notably, AKR1D1 exclusively generates the reduced steroid bearing a thermodynamically less favorable 5β-configuration. Moreover, the enzyme reduces only the Δ^4-ene, leaving the 3-oxo group intact. Thus, AKR1D1 catalyzes a reaction that is unique in steroid enzymology, and it accomplishes this with ease in comparison with chemical methods.

Rat Δ^4-3-ketosteroid 5β-reductase (AKR1D2) was first purified to homogeneity from liver as a 37-kDa protein (6). The cDNA for the corresponding human enzyme was cloned but characterized only in mammalian cell expression assays (3, 12). Recently, this enzyme has been cloned and expressed in *Escherichia coli* and completely characterized (13). These studies showed that a single enzyme could catalyze the reduction of C_{18-27} Δ^4-3-ketosteroids, yielding the corresponding 5β-dihydrosteroids. This enzyme thus plays an important role in the biosynthesis of bile acids (14, 15). For example, AKR1D1 reduces Δ^4-cholesten-7α-ol-3-one and Δ^4-cholesten-7α,12α-diol-3-one to 5β-cholestan-7α-ol-3-one and 5β-cholestan-7α,12α-diol-3-one, respectively; in turn, these two 5β-dihydrosteroids yield the bile acid precursors 5β-cholestan-3α,7α-diol and 5β-cholestan-3α,7α,12α-triol in reactions catalyzed by

* This work was supported, in whole or in part, by National Institutes of Health Research Grant R01-GM56838 (to D. W. C.) and Grants R01-DK47015 and P30-ES013508 (to T. M. P.). The costs of publication of this article were defrayed in part by the payment of page charges. This article must therefore be hereby marked "*advertisement*" in accordance with 18 U.S.C. Section 1734 solely to indicate this fact.

This paper is dedicated to Dr. Paul Talalay, The John Jacob-Abel Distinguished Service Professor, Department of Pharmacology and Molecular Sciences, Johns Hopkins School of Medicine, in honor of his 85th birthday. Paul has been a pioneer in steroid hormone enzymology throughout his career.

◆ This article was selected as a Paper of the Week.

[S] The on-line version of this article (available at http://www.jbc.org) contains supplemental Tables S1 and S2.

The atomic coordinates and structure factors (code 3BUR, 3CMF, 3COT, 3BUV, and 3BV7) have been deposited in the Protein Data Bank, Research Collaboratory for Structural Bioinformatics, Rutgers University, New Brunswick, NJ (http://www.rcsb.org/).

[1] To whom correspondence may be addressed: Dept. of Pharmacology, University of Pennsylvania, 130C John Morgan Bldg., 3620 Hamilton Walk, Philadelphia, PA 19104-6084. Tel.: 215-898-9445; Fax: 215-573-2236; E-mail: penning@pharm.med.upenn.edu.

[2] To whom correspondence may be addressed. Tel.: 215-898-5714; Fax: 215-573-2201; E-mail: chris@sas.upenn.edu.

[3] The abbreviation used is: AKR, aldo-keto reductase.

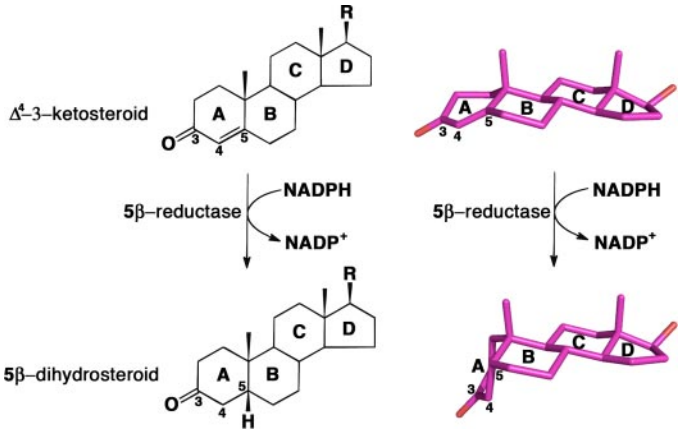

FIGURE 1. **Reduction of the carbon–carbon double bond at C-5 of a Δ⁴-3-ketosteroid to form a 5β-dihydrosteroid as catalyzed by AKR1D1.** Steroid rings and selected carbon atoms are labeled according to standard steroid nomenclature. The structures of testosterone and 5β-dihydrotestosterone (R = OH) illustrate the remarkable configurational differences between the substrate and product of this reaction (atomic coordinates retrieved from Cambridge Structural Database entries TESTOM and JEPJET, respectively) (41).

3α-hydroxysteroid dehydrogenases that belong to the same gene family, AKR1C1–AKR1C4 (4, 15–17). Subsequent oxidation of the side chain of 5β-cholestan-3α,7α-diol and 5β-cholestan-3α,7α,12α-triol yields the primary bile acids chenodeoxycholate and cholic acid, respectively.

AKR1D1 deficiency results in accumulation of C_{27} bile acid precursors bearing intact Δ⁴-3-oxo groups, which, upon reduction by steroid 5α-reductase, can be converted to *allo*-bile acids (15, 18). These sterols are hepatotoxic, and their accumulation causes liver failure (19). Steroid 5β-reductase deficiency, which is characterized by single point mutations in the enzyme (L106F, P198L, P133R, and R261C) (20–22), is effectively treated with oral bile acid therapy (19). However, the effects of these mutations on enzyme structure and function remain to be delineated.

To date, the crystal structures of many of the human AKRs have been reported, including aldehyde reductase (AKR1A1) (23) and aldose reductase (AKR1B1) (24). The structures of relevant hydroxysteroid dehydrogenases (AKR1C1–AKR1C4) have also been reported: AKR1C1, human 20α-hydroxysteroid dehydrogenase (25); AKR1C2, rat and human type III 3α-hydroxysteroid dehydrogenase/bile acid-binding protein (26, 27); AKR1C3, human type II 3α-hydroxysteroid dehydrogenase and type V 17β-hydroxysteroid dehydrogenase/prostaglandin F synthase (28); AKR1C4, human 3α-hydroxysteroid dehydrogenase type I (Protein Data Bank code 2FVL)[4]; AKR1C5, rabbit 20α-hydroxysteroid dehydrogenase type 3 (30); and AKR1C9, rat liver 3α-dihydroxysteroid dehydrogenase (31–33). Even though these hydroxysteroid dehydrogenases share significant amino acid sequence identity, these crystal structures illuminate the roles of specific residues that contribute to the differing substrate specificities among these enzymes. All AKR structures to date contain a conserved catalytic tetrad of Tyr[55], Lys[84], His[117], and Asp[50] (numbering scheme based on AKR1C9, rat 3α-hydroxysteroid dehydrogenase). In contrast, AKR1D1 is the only AKR to have a modified catalytic tetrad: His[117] is replaced by Glu[120] and is proposed to play an important role in AKR1D1 catalysis (34). In addition to the above-mentioned hydroxysteroid dehydrogenase structures, the crystal structure of a novel short chain dehydrogenase/reductase, 5β-reductase from *Digitalis lanata*, has been reported recently (35). However, this reductase is unrelated in that it adopts a Rossmann fold.

Here, we report the first x-ray crystal structure of a mammalian steroid hormone carbon–carbon double bond reductase, human Δ⁴-3-ketosteroid 5β-reductase (AKR1D1). We have determined the structures of AKR1D1 complexed with $NADP^+$ at 1.79-Å resolution, $NADP^+$ and cortisone at 1.90-Å resolution, $NADP^+$ and progesterone at 2.03-Å resolution, and $NADP^+$ and testosterone at 1.62-Å resolution. Additionally, we report the crystal structures of the binary complex with $NADP^+$ at 1.35-Å resolution (containing a HEPES buffer molecule bound in the active site). These structures provide valuable inferences regarding the catalytic mechanism and also illuminate the possible effects of single point mutations responsible for bile acid deficiency.

EXPERIMENTAL PROCEDURES

Materials—The vectors pET16b and pET28a were purchased from Novagen. *E. coli* strain C41(DE3) was provided by Dr. J. E. Walker (Medical Research Council Laboratory of Molecular Biology, Cambridge, UK). The QuikChange II site-directed mutagenesis kit was purchased from Stratagene. Restriction endonucleases were purchased from New England Biolabs. Synthetic oligonucleotides were obtained from Invitrogen. NADPH was obtained from Roche Applied Science. Steroids were purchased from Steraloids, Inc. [4-^{14}C]Testosterone (50 mCi/mmol) was obtained from PerkinElmer Life Sciences. Nickel-Sepharose 6 Fast Flow was purchased from Amersham Biosciences. All other reagents were of ACS quality or higher.

Construction of Expression Vectors—Previously, we reported the purification and characterization of recombinant AKR1D1 expressed from a pET16b vector (13). This enzyme was refractory to crystallization, and therefore, a different expression vector was generated. The pET16b-AKR1D1 expression vector was digested with NdeI and BamHI to remove the cDNA for AKR1D1. The resultant fragment was subcloned into the expression vector pET28a. The AKR1D1 insert was verified by dideoxy sequencing.

The expression vectors for AKR1D1(Y58F) and AKR1D1 (E120A) were made using the pET16b-AKR1D1 construct as a template by conducting site-directed mutagenesis using the QuikChange method following the manufacturer's protocol. The following forward and reverse primers were used (where the boldface nucleotides indicate the mutation introduced): for the Y58F mutant, 5′-dGGG GCC TAC ATC T**T**C CAA AAT GAA CAC GAA GTT GG-3′ and 5′-dCC AAC TTC GTG TTC ATT TTG G**A**A GAT GTA GGC CCC-3′; and for the E120A mutant, 5′-dG GAT CTT TAC ATC ATT G**C**A GTA CCA ATG GCC TTT AAG C-3′ and 5′-dG CTT AAA GGC CAT TGG T**A**C TGC AAT GAT GTA AAG ATC C-3′. The intro-

[4] E. Ugochukwu, C. Smee, K. Guo, P. Lukacik, K. Kavanagh, J. E. Debreczeni, F. von Delft, J. Weigelt, M. Sundstrom, C. Arrowsmith, A. Edwards, and U. Oppermann, unpublished data.

duction of these mutations into the pET16b-AKR1D1 construct was verified by dideoxy sequencing.

Expression and Purification of AKR1D1—The pET28a-AKR1D1 expression vector was used to transform competent *E. coli* C41(DE3) cells. The cells were grown in 4-liter cultures of Luria-Bertani medium at 37 °C (containing 100 μg/ml ampicillin). Upon reaching A_{600} = 0.6, 1 mM isopropyl 1-thio-β-D-galactopyranoside was added to induce enzyme expression overnight. The following day, the culture was centrifuged for 15 min at 10,000 × *g*, and the pellets were resuspended in 20 mM Tris-HCl (pH 7.9) and 5 mM imidazole. Resuspensions were lysed by sonication and centrifuged for 15 min at 10,000 × *g*, and the supernatant was dialyzed overnight in 20 mM Tris-HCl (pH 7.9), 20 mM imidazole, and 0.5 M NaCl. The dialyzed fraction was loaded onto a nickel-Sepharose column equilibrated with the dialysis buffer, and the column was washed with the same buffer. Bound protein was eluted with a linear gradient of 20–400 mM imidazole. Active fractions containing AKR1D1 were identified by monitoring the conversion of [4-^{14}C]testosterone to 5β-dihydrotestosterone by discontinuous assay using standard assay conditions and by visualization of the protein content of each fraction by SDS-PAGE. Peak fractions were pooled and dialyzed overnight in 20 mM Tris-HCl (pH 7.0) containing 1 mM EDTA. The final specific activity of the recombinant enzyme was 80 nmol of testosterone reduced per min/mg. The mutant proteins AKR1D1(Y58F) and AKR1D1(E120A) were purified in a similar manner.

Standard Radiometric Assay—The reduction of [4-^{14}C]testosterone was used to monitor 5β-reductase activity collected during purification and for activity measurements. Reactions contained 2 μM [4-^{14}C]testosterone (40,000 dpm), 8 μM unlabeled testosterone, 5% acetonitrile, and 100 mM potassium phosphate buffer (pH 6.0). Reactions were initiated by the addition of 200 μM NADPH and performed at 37 °C. The substrate and product of the quenched reaction were separated by TLC and quantitated by scintillation counting.

Crystallography—The ternary complexes of AKR1D1·$NADP^+$·testosterone, AKR1D1·$NADP^+$·cortisone, AKR1D1·$NADP^+$·progesterone, and AKR1D1·$NADP^+$·HEPES were crystallized by the hanging drop vapor diffusion method at 4 °C. In a typical experiment, drops containing 4.0 μl of enzyme solution (5.0 mg/ml AKR1D1, 2.0 mM $NADP^+$, 2.0 mM steroid, and 10.0 mM Tris (pH 7.4)) and 4.0 μl of precipitant buffer (0.1 M HEPES/Tris-HCl (pH 7.0), 10–20% (w/v) polyethylene glycol 4000, and 10% isopropyl alcohol) were equilibrated against a 1-ml reservoir of precipitant buffer. Diamond-like crystals appeared in ~2–3 days with typical dimensions of 0.2 × 0.3 × 0.5 mm. Crystals of each AKR1D1·$NADP^+$·steroid complex were further soaked for 1 week in the same mother liquor solution augmented with 5.0 mM $NADP^+$ and 5.0 mM steroid to ensure complete ligand occupancy. Following transfer to a 28% glycerol cryoprotectant solution and flash-cooling, crystals of the AKR1D1·$NADP^+$·testosterone complex yielded diffraction data to 1.62-Å resolution at the Advanced Light Source (beamline 8.2.2, λ = 1.000 Å, 100 K). Diffraction intensities measured from these crystals indicated a space group $P2_12_12_1$ with unit cell parameters a = 49.8, b = 110.1, and c = 129.4 Å. There were two molecules in the asymmetric unit and the Matthews coefficient V_M = 2.4 Å^3/Da, corresponding to a solvent content of 48.5%. Crystals of the AKR1D1·$NADP^+$·cortisone, AKR1D1·$NADP^+$·progesterone, and AKR1D1·$NADP^+$·HEPES complexes yielded diffraction data to 1.90-, 2.03-, and 1.35-Å resolution, respectively, at Brookhaven National Laboratory (beamlines X6A and X29A, λ = 1.000 Å, 100 K) and were found to be isomorphous with crystals of the AKR1D1·$NADP^+$·testosterone complex (Table 1). Data reduction was achieved with HKL2000 (36) and Scalepack (36) (Table 1).

For crystallization of the AKR1D1·$NADP^+$ complex, hanging drops containing 4.0 μl of enzyme solution (5.0 mg/ml AKR1D1, 2 mM NADPH, 2.0 mM 5β-cholestan-3-one, and 10.0 mM Tris (pH 7.4)) and 4.0 μl of precipitant buffer (0.1 M Tris/HEPES (pH 7.5), 10–20% (w/v) polyethylene glycol 4000, and 10% isopropyl alcohol) were equilibrated against a 1-ml reservoir of precipitant buffer. Crystals of the AKR1D1·$NADP^+$ complex were soaked for 1 week in the same mother liquor solution augmented with 5.0 mM 5β-cholestan-3-one, a steroid product containing a *cis*-A/B-ring fusion. Following transfer to a cryoprotectant solution containing 28% glycerol, crystals of the AKR1D1·$NADP^+$ complex yielded diffraction data to 1.80-Å resolution at the Advanced Photon Source (beamline 22 BM, λ = 1.000 Å, 100 K) and were isomorphous with crystals of the ternary complexes discussed above (Table 1).

The structure of the AKR1D1·$NADP^+$·testosterone complex was solved by molecular replacement using one monomer of the AKR1C2·$NADP^+$·testosterone complex (Protein Data Bank code 1J96) (27) less the atoms of $NADP^+$·testosterone and solvent as an initial search probe. The program PHASER (37) was used to perform the molecular replacement calculations; the optimal solution for the positioning of the two monomers in the asymmetric unit yielded a total log likelihood gain of 1832, a rotation function Z score of 12.3, and a translational function Z score of 19.5 for the first monomer and a rotation function Z score of 13.2 and a translational function Z score of 42.5 for the second monomer using data in the 50-2.5-Å resolution range. The analysis of this solution showed reasonable packing interactions in the unit cell. The initial electron density map clearly revealed the presence of $NADP^+$ bound in the active site. Using the programs O (38) and CNS (39) for model fitting and refinement, respectively, the model was manually rebuilt and refined. In the later stages of refinement with CNS, the non-crystallographic symmetry restraints were released, after which the program SHELX was used to complete the refinement (40). Additional solvent molecules were introduced during refinement with SHELX, and the electron density map of testosterone became very clearly defined. In the final stage of refinement, the atomic coordinates of testosterone were retrieved from entry TESTOM in the Cambridge Structural Database (41), built into the electron density map, and refined with full occupancy. The quality of the final model was checked with Verify3d (42); the analysis of the structure was performed with PISA (43).

The crystal structures of the AKR1D1·$NADP^+$·cortisone, AKR1D1·$NADP^+$·progesterone, AKR1D1·$NADP^+$·HEPES, and

TABLE 1

Data collection and refinement statistics

PDB, Protein Data Bank; r.m.s., root mean square.

Structure	AKR1D1·NADP⁺· testosterone complex	AKR1D1·NADP⁺· cortisone complex	AKR1D1·NADP⁺· progesterone complex	AKR1D1·NADP⁺· HEPES complex	AKR1D1· NADP⁺ complex
Data collection					
PDB code	3BUR	3CMF	3COT	3BUV	3BV7
Resolution range (Å)	50.0–1.62	50.0–1.90	30.0–2.03	50.0–1.35	50.0–1.79
Unique reflections measured	86,037 (7,952)	51,994 (4,640)	44,101 (4,301)	147,700 (13,665)	66,774 (6,684)
R_{merge} [a]	0.103 (0.36)[b]	0.112 (0.50)[b]	0.131 (0.58)[b]	0.094 (0.41)[b]	0.109 (0.39)[b]
$I/\sigma(I)$	20.3 (2.7)[b]	10.9 (2.5)[b]	12.2 (2.0)[b]	22.6 (1.9)[b]	20.5 (3.4)[b]
Completeness (%)	96.0 (90.0)[b]	93.7 (84.9)[b]	97.6 (96.9)[b]	95.7 (89.6)[b]	98.6 (100.0)[b]
Refinement statistics					
Reflections used in refinement (test set)	81,663/4,306	49,006/2,451	41,289/1,866	140,579/7,075	63,520/2,800
R/R_{free} [c]	0.228/0.248	0.195/0.223	0.194/0.234	0.218/0.232	0.236/0.257
Protein atoms[d]	5,254	5,254	5,254	5,254	5,254
Water molecules[d]	498	616	497	556	304
NADP⁺ molecules[d]	2	2	2	2	2
Glycerol molecules[d]	10			2	3
Testosterone molecules[d]	2				
Cortisone molecules[d]		2			
Progesterone molecules[d]			2		
HEPES molecules[d]				1	
r.m.s. deviations					
Bond lengths (Å)	0.007	0.006	0.007	0.005	0.012
Bond angles	1.1°	1.2°	1.1°	1.2°	1.1°
Average *B*-factors (Å²)					
Main chain atoms	17	15	26	16	20
Side chain atoms	22	17	28	19	25
Water molecules	31	27	35	26	25
NADP⁺	14	10	20	12	16
Testosterone	34				
Cortisone		41			
Progesterone			54		
HEPES				34	
Glycerol	42			43	41
Ramachandran statistics[e]					
Allowed (%)	90.4	89.2	89.0	89.9	91.1
Additionally allowed (%)	9.3	10.5	10.7	9.8	8.6
Generously allowed (%)	0.0	0.3	0.3	0.2	0.2
Disallowed (%)	0.2	0.0	0.0	0.2	0.2

[a] $R_{merge} = \Sigma|I - \langle I\rangle|/\Sigma I$, where I is the observed intensity and $\langle I\rangle$ is the average intensity calculated for replicate data.
[b] The number in parentheses refer to the outer 0.1-Å shell of data.
[c] Crystallographic *R*-factor, $R = \Sigma(||F_o| - |F_c||)/\Sigma|F_o|$ for reflections contained in the working set. Free *R*-factor, $R_{free} = \Sigma(||F_o| - |F_c||)/\Sigma|F_o|$ for reflections contained in the test set excluded from refinement. $|F_o|$ and $|F_c|$ are the observed and calculated structure factor amplitudes, respectively.
[d] Per asymmetric unit.
[e] Ramachandran statistics were calculated with PROCHECK (29).

AKR1D1·NADP⁺ complexes were solved by the difference Fourier method. Refinement was performed as described above using CNS (39).

Twenty-one residues at the N terminus (the uncleaved expression tag from the pET28a vector) were disordered and therefore excluded from the final model of each structure. The exclusion of 21 of 346 residues in each monomer (6.1% of the scattering matter) likely contributed to the slightly elevated *R* and R_{free} values recorded in Table 1.

RESULTS

Crystal Structure of the AKR1D1·NADP⁺ Complex—The asymmetric unit of the unit cell contains two monomers of AKR1D1. Each monomer consists of a 325-residue polypeptide chain that adopts an $(\alpha/\beta)_8$-barrel fold typical of AKRs. The top of the β-barrel is capped by loops A (Ile^{119}–Leu^{147}), B (Tyr^{219}–Leu^{238}), and C (Leu^{302}–Tyr^{326}), which enclose the active site (Fig. 2*a*). Notably, the Pro^{133}–Lys^{139} segment in loop A of monomer A exhibits higher thermal *B*-factors compared with the Pro^{133}–Lys^{139} segment in monomer B, where this segment appears to be stabilized in part by interlattice contacts. However, the loop A conformations in monomers A and B are essentially identical (data not shown).

Given the amino acid sequence identities of 56% between AKR1D1 and AKR1C2 (27) and 58% between AKR1D1 and AKR1C9 (33), the overall tertiary structures of these enzymes are quite similar. The root mean square deviation of 307 C-α atoms between AKR1D1 in complex with NADP⁺ and between AKR1C2 in complex with NADP⁺ and testosterone (Protein Data Bank Code 1J96) (27) is 1.0 Å, and that of 317 C-α atoms between AKR1D1 and AKR1C9 complexed with NADP⁺ and testosterone (Protein Data Bank code 1AFS) is 0.78 Å (33). However, significant conformational differences in loops A, B, and C are observed when the structures of AKR1D1, AKR1C2, and AKR1C9 are compared (Fig. 2*b*). The majority of amino acid substitutions between AKR1D1 and these enzymes are found in these loops. The Val^{309}–Phe^{322} segment of loop C and its corresponding segment in AKR1C2 exhibit significant C-α deviations of ~4 Å. Because these loops play an important role in substrate binding, it is likely that their sequence and structural differences reflect differences in steroid substrate specificity and catalysis among these enzymes.

The NADP⁺ cofactor in the AKR1D1·NADP⁺ complex adopts an extended *anti*-conformation as observed in other

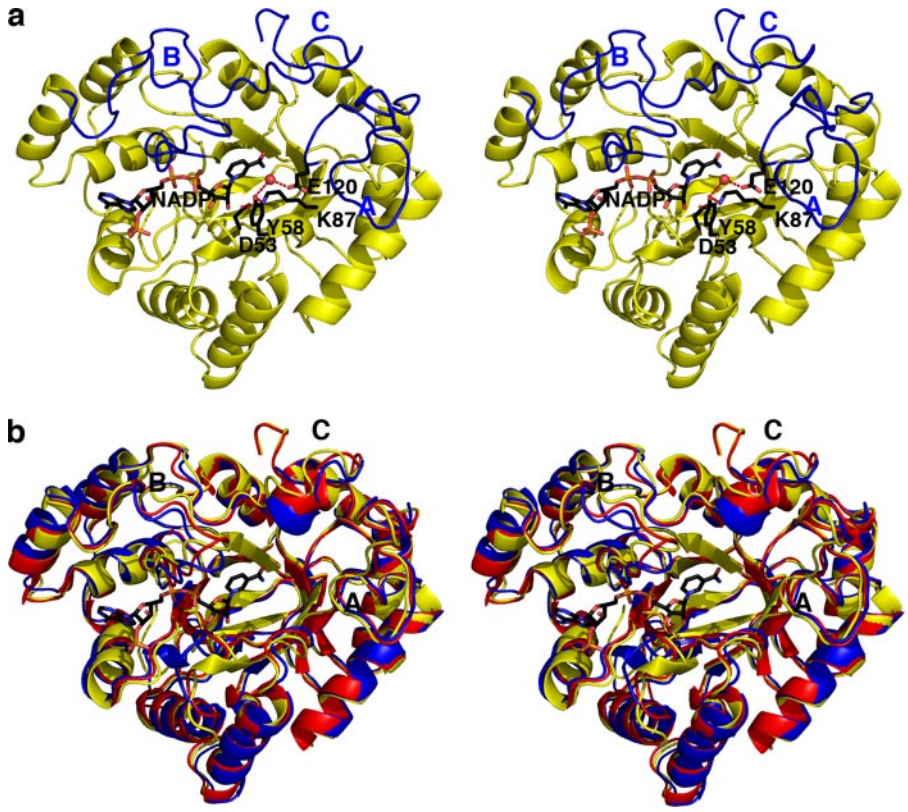

FIGURE 2. **AKR1D1·NADP⁺ complex.** *a*, AKR1D1 adopts the $(\alpha/\beta)_8$-barrel fold conserved among members of the AKR superfamily. Loops A, B, and C (*blue*) flank the steroid-binding pocket. Atoms of the catalytic tetrad and NADP⁺ are labeled and color-coded as follows: carbon, *black*; oxygen, *red*; and nitrogen, *blue*. The water molecule hydrogen-bonded between Tyr[58] and Glu[120] is indicated by a *red sphere*. Hydrogen bonds are indicated by *red dashed lines*. *b*, superposition of AKR1D1 (*yellow*), AKR1C9 (*red*), and AKR1C2 (*blue*) reveals significant conformational differences in loops A, B, and C.

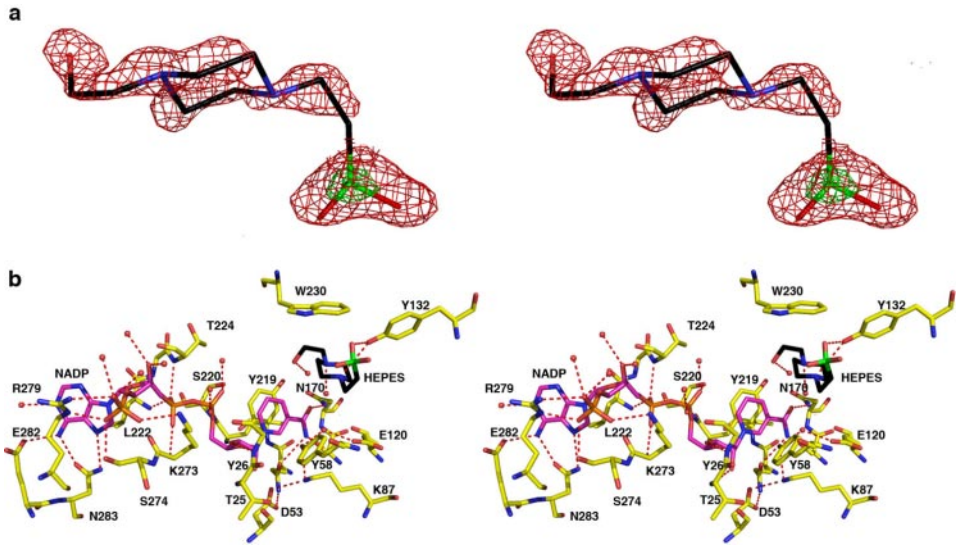

FIGURE 3. **AKR1D1·NADP⁺·HEPES complex.** *a*, shown is the difference electron density map of HEPES bound in the active site of AKR1D1 prior to the inclusion of HEPES in the refinement (contoured at 2.2σ; *red*). The electron-rich sulfur atom of HEPES is indicated by its stronger electron density contoured at 6.7σ (*green*). *b*, hydrogen bond interactions in the AKR1D1·NADP⁺·HEPES complex are indicated by *red dashed lines*. Atoms are color-coded as described for Fig. 2*a* except that protein carbon atoms are *yellow*, HEPES carbon atoms are *black*, and its sulfur atom is *green*.

AKR structures and is located in a long tunnel with the adenine group exposed to solvent and the nicotinamide ring located deep inside the tunnel oriented toward the central active site cavity (Fig. 2*a*). Approximately 84% of the accessible surface area of NADP⁺ is buried inside the tunnel. The NADP⁺ cofactor participates in a significant number of hydrogen bond interactions (Fig. 3). Notably, the cofactor binding mode is essentially conserved with respect to that observed in AKR1C9 (32) or AKR1C2 (27). In complex with AKR1D1, the nicotinamide headgroup of NADP⁺ is stacked against Tyr[219], and the carboxamide group makes contacts with Asn[170], Ser[169], and Gln[193]. Additionally, the phosphate group of 2′-AMP makes an electrostatic link with Arg[279]. However, these structures do not reveal a hydrogen bond interaction between Asn[227] and Lys[30] and Lys[273] that would correspond to the salt link interaction between Asp[217] and Lys[22] and Lys[263] observed in the AKR1A1 structure (23) or the salt link interactions between Asp[216] and Lys[21] and Lys[262] observed in the AKR1B1 structure (24). These salt links create a "safety belt" that contributes to the high affinity (~10 nM) of cofactor binding to AKR1A1 and AKR1B1. Because NADP⁺ binding to AKR1D1 lacks this safety belt, binding affinity should be weaker and more comparable with cofactor binding to AKRs similarly lacking a safety belt (100–200 nM), and this is what has been observed (13).

Interestingly, when crystals of the AKR1D1·NADP⁺ complex were grown in the presence of 5β-cholestan-3-one, the binding of this product-like steroid containing a *cis*-A/B-ring fusion was not observed. Instead, either a molecule of glycerol from the cryoprotectant solution bound in the active site of monomer A (1.79-Å resolution structure) (data not shown), or a HEPES molecule from the crystallization buffer bound in the active site of monomer B (1.35-Å resolution structure) (Fig. 3). Thus, these two structures represent those of the binary AKR1D1·NADP⁺ complex.

Crystal Structures of the AKR1D1·NADP⁺·Cortisone and AKR1D1·NADP⁺·Progesterone Complexes—In these enzyme·substrate complexes, the electron density of each steroid substrate is clear and unambiguous (Fig. 4, *a* and *b*), showing

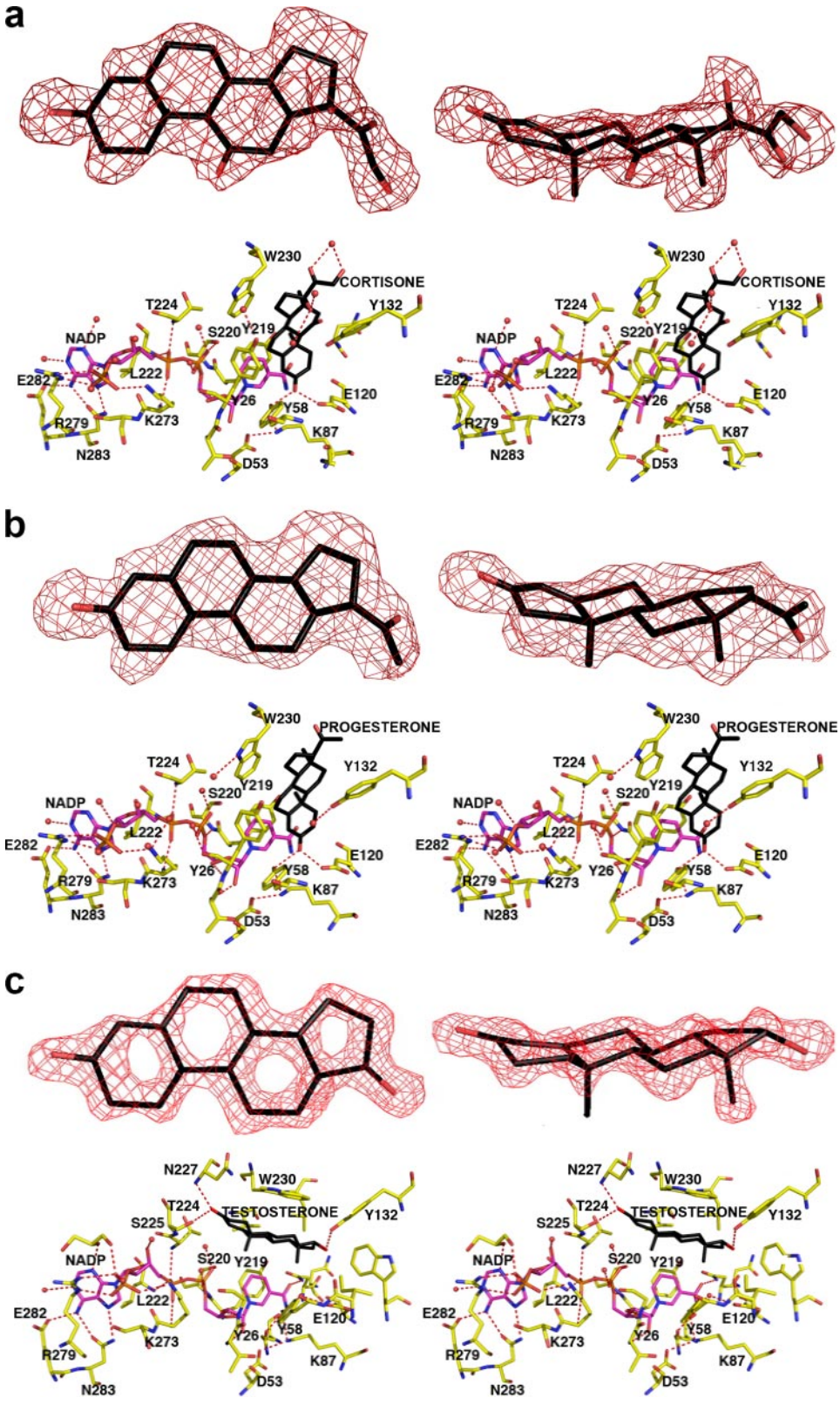

FIGURE 4. **AKR1D1·NADP⁺-steroid complexes.** Two map orientations are shown for each steroid, and hydrogen bond interactions are indicated by *red dashed lines*. Atoms are color-coded as described for Fig. 2*a* except that protein carbon atoms are *yellow*. For clarity, the orientation of the protein is rotated ~180° horizontally relative to the orientation shown in Fig. 2*a*. *a*, difference electron density map of cortisone contoured at 2.7σ. *b*, difference electron density map of progesterone contoured at 2.6σ. *c*, difference electron density map of testosterone contoured at 2.3σ. Note the dramatically different, nonproductive binding mode of testosterone; in contrast with the binding of cortisone and progesterone, the A-ring of testosterone is oriented away from the catalytic tetrad and the nicotinamide ring of the cofactor.

that each steroid lies perpendicular to the $NADP^+$ cofactor. The binding of cortisone is very similar to the binding of progesterone even though these steroids bear different pendant groups on their D-rings.

Overall, the crystal structure of each ternary complex is very similar to that of the AKR1D1·$NADP^+$ complex, with root mean square deviations of 0.26 and 0.13 Å, respectively, for 325 C-α atoms. However, important conformational differences are evident in loops A and B. Significantly, cortisone and progesterone binding triggers the movement of Ser^{225}–Val^{231} in loop B away from the active site, with C-α deviations ranging from 0.3 to 2 Å. Furthermore, an ~7-Å movement of the side chain of Trp^{230} accommodates substrate binding (illustrated for cortisone binding in Fig. 5). Thus, Trp^{230} appears to play a key role in packing against the β-face of the steroid ring system in the active site of human AKR1D1, as also observed for the corresponding tryptophan residue in the structure of the AKR1C9·$NADP^+$·testosterone complex (33).

In the AKR1D1 active site, ~80% of the accessible surface area of each steroid substrate is buried in the hydrophobic binding pocket. Each steroid substrate is positioned with its β-face oriented toward the *re*-face of the nicotinamide ring of $NADP^+$ such that the steroid carbon–carbon double bond would be adjacent to the 4-pro-(*R*)-hydrogen of NADPH (Fig. 4, *a* and *b*). The C-3 carbonyl oxygen of each steroid substrate accepts hydrogen bonds from the phenolic hydroxyl group of Tyr^{58} and the *anti*-oriented conformer of the carboxylic acid side chain of Glu^{120}. Notably, the C-3 carbonyl oxygen of each substrate occupies the same position as the water molecule that hydrogen bonds with Tyr^{58} and Glu^{120} in the AKR1D1·$NADP^+$ complex (Figs. 2 and 3). Site-directed mutagenesis of these residues to Y58F and E120A supports their role in catalysis

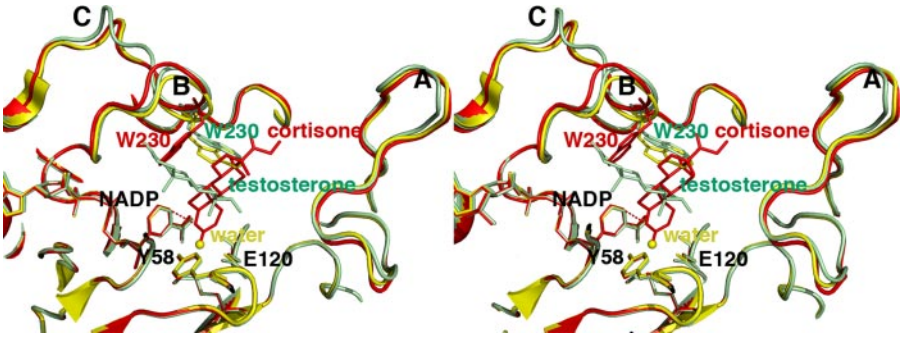

FIGURE 5. **Least-squares superposition of the AKR1D1·NADP$^+$ (*yellow*), AKR1D1·NADP$^+$·cortisone (*red*), and AKR1D1·NADP$^+$·testosterone (*green*) complexes.** The distance of ~3.7 Å between the anomeric carbon of NADP$^+$ and the olefinic C-4 of cortisone is indicated by a *red dashed line*, which would represent the trajectory of hydride transfer from NADPH. The position of the water molecule in the unliganded structure is indicated by a *yellow sphere*. Loops A, B, and C are labeled; note that loop B and Trp^{230} in particular must undergo a significant conformational change to accommodate productive substrate binding as represented by cortisone (*red*). The indole ring of Trp^{230} remains in its substrate-free conformation (*yellow*) to accommodate the nonproductive binding mode of testosterone (*green*).

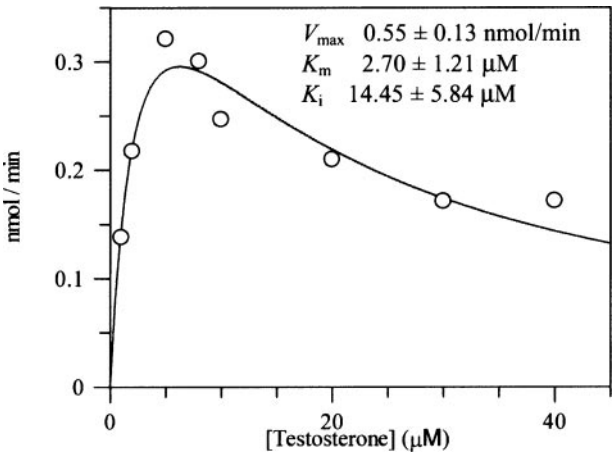

FIGURE 6. **Substrate inhibition of AKR1D1 by testosterone.** A velocity *versus* substrate plot for AKR1D1 shows substrate inhibition using testosterone. Assays contained 0.078 μM enzyme, 1–40 μM testosterone, 15 μM NADPH, and 4% acetonitrile in 100 mM potassium phosphate buffer (pH 6.0) in a final volume of 1 ml. Reactions were monitored fluorometrically using an excitation wavelength of 340 nm (slit width of 5 nm) and an emission wavelength of 450 nm (slit width of 10 nm) at 37 °C. Kinetic analysis of initial velocities obtained was performed using the Henri-Michaelis-Menten equation for uncompetitive substrate inhibition, $v = (V_{max} \times [S])/(K_m + [S] + [S]^2/K_i)$, and fit using the program GraFit. The iterative fits provided estimates of V_{max}, K_m, and K_i and associated S.E. values.

because neither mutant has any detectable activity in the reduction of testosterone using the standard radiometric assay, where the limit of detection is 0.002 nmol/min.

Crystal Structure of the AKR1D1·NADP$^+$·Testosterone Complex—In this enzyme·substrate complex, the electron density of testosterone is extremely well defined. However, the arrangement of NADP$^+$ and testosterone differs from that seen in the other ternary complexes because they are parallel and not perpendicular. Testosterone also binds with a "backward" orientation in which its D-ring binds in the same region occupied by the A-rings of cortisone and progesterone in their respective complexes with AKR1D1 (Fig. 4*c*). Consequently, the carbon–carbon double bond of testosterone is distant from the nicotinamide ring of the cofactor, and this binding orientation is judged to be nonproductive. The side chain of Trp^{230} does not undergo a conformational change to accommodate testosterone binding and instead remains in the conformation observed in the structure of the substrate-free AKR1D1·NADP$^+$ complex (Fig. 5). Approximately 85% of the accessible surface area of testosterone is buried in the hydrophobic binding pocket. The testosterone C-3 carbonyl group accepts hydrogen bonds from Asn^{227} and Ser^{225}, whereas the testosterone hydroxyl group makes a hydrogen bond interaction with Tyr^{132}.

The nonproductive testosterone binding modes observed with AKR1C2 and AKR1D1 suggest that this particular steroid can occupy more than one position and that at the high steroid concentrations used in the crystallization trials, the nonproductive binding mode is favored. This is reflected in substrate inhibition observed with AKR1C2 (44, 45). We also observed substrate inhibition of AKR1D1 by high concentrations of testosterone. Although the K_m value for this steroid is close to 2.0 μM, concentrations of testosterone that exceed 10 μM produced marked inhibition (Fig. 6).

Disease-linked Mutations—Four point mutations in AKR1D1 are associated with bile acid deficiency: L106F, P198L, P133R, and R261C (20–22). As predicted from other AKR structures, these residues are not located in the cofactor- or steroid-binding sites and are not involved in catalysis. The locations of these residues in the AKR1D1 structure are shown in Fig. 7. The P133R substitution in loop A is closest to the substrate-binding site, and it is conceivable that this substitution perturbs the conformational changes in loop A that accompany steroid binding. The remaining mutations may exert a deleterious effect on catalysis by causing structural changes that propagate through the protein scaffold to perturb substrate and/or cofactor binding or by otherwise destabilizing the folded conformation of the protein.

DISCUSSION

The x-ray crystal structure of human Δ⁴-3-ketosteroid 5β-reductase (AKR1D1) is the first structure of a mammalian steroid carbon–carbon double bond reductase. As a member of the AKR superfamily, it is not surprising that the $(\alpha/\beta)_8$-barrel fold and the NADP$^+$ cofactor-binding site of AKR1D1 are highly conserved with those other members of the superfamily. However, the structures of AKR1D1·substrate complexes reported herein illuminate new features of steroid substrate recognition, the catalytic mechanism, and the positions of natural mutations associated with bile acid deficiency.

Substrate Recognition—AKR1D1 binds Δ⁴-3-ketosteroids productively and nonproductively. In the productive binding mode observed with cortisone and progesterone, the two substrates are bound similarly in a pocket defined by residues from the β2–α2 loop, loop A, loop B, and loop C. Alignments of pocket and loop residues of AKR1D1 with those of other AKR1C structures containing bound steroids are shown in sup-

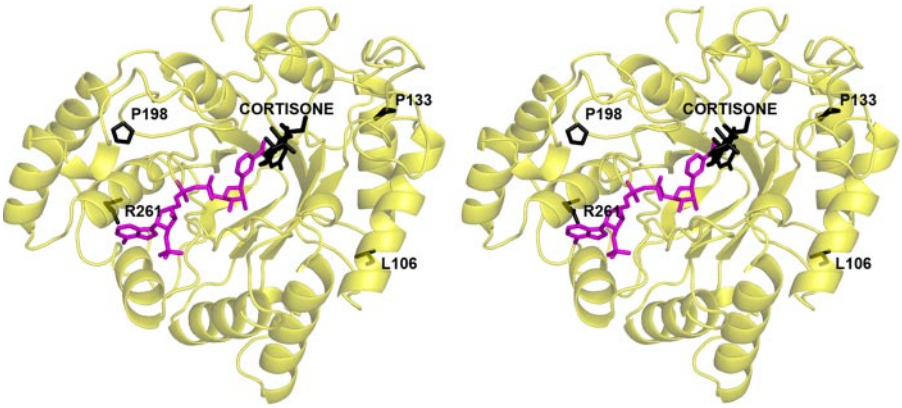

FIGURE 7. **AKR1D1·NADP⁺·cortisone complex: positions of the natural mutations L106F, P198L, P133R, and R261C.** Cortisone, Leu[106], Pro[198], Pro[133], and Arg[261] atoms are *black*, and NADP⁺ atoms are *magenta*. Among these four residues, Pro[133] in loop A is closest to the substrate-binding site.

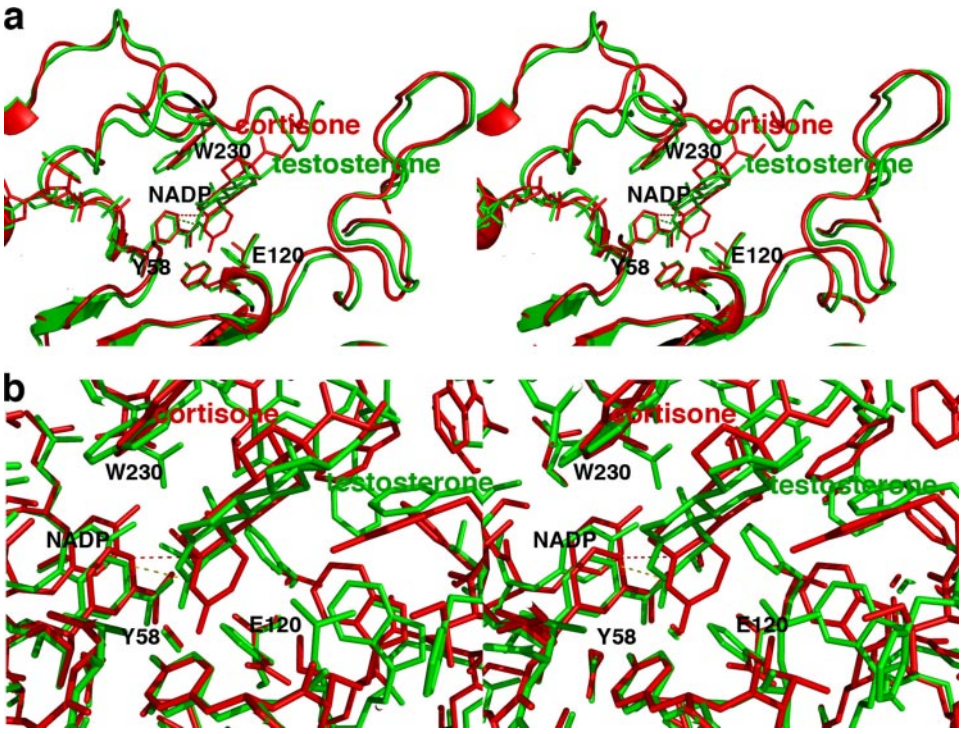

FIGURE 8. **Comparisons of steroid binding modes in catalysis.** *a*, superposition of the AKR1D1·NADP⁺·cortisone complex (*red*) on the AKR1C9·NADP⁺·testosterone complex (*green*) showing that the A-ring of the substrate binds ~1 Å deeper in the active site of the former enzyme relative to the position of the nicotinamide ring of NADP⁺. Presuming that NADPH binds similarly to NADP⁺, the 4-pro-(*R*)-hydride of NADPH would be adjacent to the substrate C-3 carbonyl in the AKR1C9 active site (*green dotted lines*), whereas the 4-pro-(*R*)-hydride of the NADPH cofactor would be adjacent to C-5 of the substrate carbon–carbon double bond in the AKR1D1 active site (*red dotted lines*). *b*, same orientation as *a*, but a close-up view showing all atoms.

plemental Tables S1 and S2. Of the 10 pocket residues assigned, Tyr[58] is catalytic, and Tyr[26] and Trp[230] are highly conserved. The indole ring of Trp[230] in the AKR1D1 structures is versatile in that rotation around both side chain torsion angles and movement of the associated polypeptide backbone of loop B allow the indole ring to pack differently, *i.e.* against the β-face of a productively bound steroid substrate or against the α-face of a nonproductively bound steroid substrate (Fig. 5).

Interestingly, superposition of the AKR1D1·NADP⁺·cortisone and AKR1C9·NADP⁺·testosterone complexes, in which both substrates adopt productive binding orientations, reveals that the substrate is immobilized more deeply in the active site of AKR1D1 compared with AKR1C9 (Fig. 8). In part, this appears to result from the removal of the steric bulk of the His[120] imidazole side chain by the substitution of Glu[120] in AKR1D1. As a result, the 4-pro-(*R*)-hydride of the NADPH cofactor would be adjacent to the substrate C-3 carbonyl group in the AKR1C9 active site, and the 4-pro-(*R*)-hydride of the NADPH cofactor would be adjacent to C-5 of the substrate carbon–carbon double bond in the AKR1D1 active site (Fig. 8).

Catalytic Mechanism—The four catalytic residues Asp[53], Tyr[58], Lys[87], and Glu[120] are located in the center of the β-barrel (Fig. 2*a*). The side chain of Lys[87] donates hydrogen bonds to Asp[53] and Tyr[58]. In the substrate-free enzyme, the phenolic hydroxyl group of Tyr[58] donates a hydrogen bond to a water molecule, which in turn hydrogen bonds with Glu[120]. Because the C-3 carbonyl oxygen atoms of the substrates cortisone and progesterone displace this water molecule in their complexes with AKR1D1, the side chain of Glu[120] must be protonated as the *anti*-oriented carboxylic acid to donate a hydrogen bond to the substrate carbonyl oxygen (and possibly also the water molecule in the substrate-free enzyme). Furthermore, given that carboxylate groups that serve as general bases generally do so with their more basic, *syn*-oriented lone electron pairs (46), it is reasonable to conclude that protonated carboxylic acids that serve as general acids or hydrogen bond donors may do so with their more acidic (pK_a ~0.5) *anti*-oriented conformers. Thus, in AKR1D1, the *anti*-oriented conformer of Glu[120] may serve as a superacidic hydrogen bond donor to help activate the α,β-unsaturated ketone moiety of the substrate for carbon–carbon bond reduction by NADPH.

That Glu[120] appears in AKR1D1 represents a unique exception for AKRs having an $(\alpha/\beta)_8$-barrel fold. All other AKRs, including AKR1C9 (33) and AKR1C2 (26), have a histidine residue at the corresponding position. The side chain conformations of Asp[53], Tyr[58], and Lys[87] are mostly conserved with respect to the conformations of corresponding residues in the AKR1C2·NADP⁺·testosterone complex; the side chain of Glu[120] is coplanar with respect to the orientation of the corre-

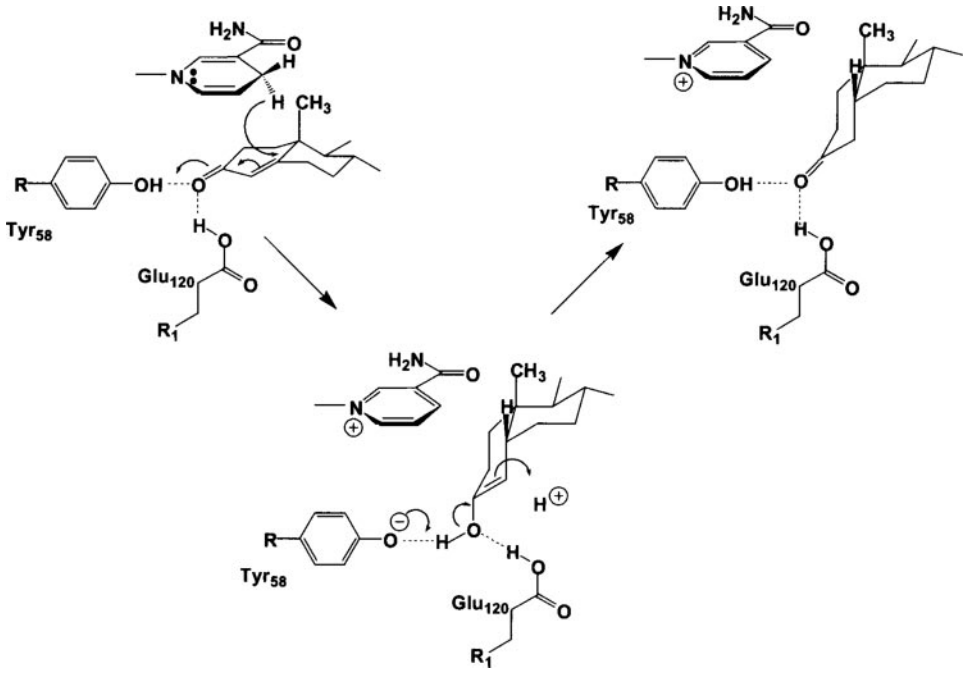

FIGURE 9. **Proposed catalytic mechanism for steroid double bond reduction.** The 4-pro-(*R*)-hydride transfer from the *re*-face of NADPH to C-5 of the Δ^4-ene is proposed while the C-3 carbonyl is polarized by both Tyr^{58} and Glu^{120}, which create a superacidic oxyanion hole as predicted by Jez and Penning (34).

sponding histidine residue in this complex (27). Interestingly, the hydrogen-bonded water molecule between Tyr^{58} and Glu^{120} occupies a position close to that of an acetate oxygen atom observed in the AKR1C2·$NADP^+$·testosterone complex (27), and a corresponding water molecule is also observed in the crystal structure of AKR1C9 (32). It is proposed that the binding of this water molecule in AKR1C9 mimics the binding of the carbonyl oxygen of a 3-ketosteroid substrate (33).

In AKR1D1, the interactions of Tyr^{58} and Glu^{120} with the carbonyl groups of steroid substrates suggest that both residues participate in the catalytic mechanism of carbon–carbon double bond reduction. In AKR1B1 and AKR1C9, site-directed mutagenesis studies provide compelling evidence that the catalytic tyrosine acts as the general acid-base (47, 48). Moreover, site-directed mutagenesis studies of AKR1C9 also show that the corresponding H117E substitution introduces 5β-reductase activity into this enzyme (34). Based on k_{cat} and k_{cat}/K_m pH-rate profiles for wild-type AKR1C9 and AKR1C9(H117E) enzymes, a facilitatory role for the glutamic acid residue is proposed in which it alters the pK of Tyr^{55}, which functions as the general acid. This facilitatory role is based on an acid shift in the pK_b of Tyr^{55} in the H117E mutant. These data are interpreted to indicate that Tyr^{55} has more $TyrOH_2^+$ character (*i.e.* it may behave as a "superacid"), which in turn polarizes the α,β-unsaturated ketone so that hydride transfer can occur at C-5.

The carboxylic acid side chain of Glu^{120} may also serve as a superacid to help polarize the C-3 ketone of a productively bound substrate such as cortisone or progesterone (Fig. 4, *a* and *b*). The non-enzymatic mechanism of carbon–carbon double bond reduction in an α,β-unsaturated ketone requires a superacid such as HF-SbF_5 (49), and it is possible that AKR1D1 adopts a similar strategy for catalysis. Generation of the AKR1D1(Y58F) and AKR1D1(E120A) mutants abolishes all enzyme activity, consistent with the crucial role of these residues in catalysis. Once 4-pro-(*R*)-hydride transfer from the *re*-face of NADPH to the carbon–carbon double bond of the substrate is achieved, the substrate will adopt a bent, *cis*-A/B-ring conformation. Either an enzyme-bound residue or a solvent molecule will protonate the C-4 atom of the substrate in the final step of the steroid reduction reaction. A proposed mechanism that incorporates these structural data in light of available enzymological measurements is presented in Fig. 9.

Disease-linked Mutations—The four point mutations associated with inherited bile acid deficiency are located in regions independent of substrate recognition and catalysis. If these mutations are responsible for bile acid deficiency, then it is likely that they affect conformational changes in loop A that accompany substrate binding (P133R) and/or otherwise compromise enzyme stability. Future studies of these mutant recombinant proteins and their expression in mammalian cells will allow us to probe the structural and functional consequences of these mutations.

Acknowledgments—We thank the Brookhaven National Laboratory (beamlines X6A, X12B, and X29A; Upton, NY), the Advanced Light Source (beamline 8.2.2; Berkeley, CA), and the Advanced Photon Source (beamline 22 BM, Chicago, IL) for beamtime access.

REFERENCES

1. Tomkins, G. (1956) *Recent Prog. Horm. Res.* **12,** 125–133
2. Russell, D. W., and Wilson, J. D. (1994) *Annu. Rev. Biochem.* **63,** 25–61
3. Kondo, K.-H., Kai, M. H., Setoguchi, Y., Eggersten, G., Sjöblom, P., Setoguchi, Y., Okuda, K. I., and Björkhem, J. (1994) *Eur. J. Biochem.* **219,** 357–363
4. Jez, J. M., Bennett, M. J., Schelgel, B. P., Lewis, M., and Penning, T. M. (1997) *Biochem. J.* **325,** 625–636
5. Berséus, O., Danielsson, H., and Einarsson, K. (1967) *J. Biol. Chem.* **242,** 1211–1219
6. Okuda, K., and Okuda, K. (1984) *J. Biol. Chem.* **259,** 7519–7524
7. Onishi, Y., Noshiro, M., Shimosato, T., and Okuda, K. (1991) *FEBS Lett.* **283,** 215–218
8. Norymberski, J. K., and Woods, G. F. (1955) *J. Chem. Soc.* (*Lond.*) 3426–3430
9. March, J. (1984) in *Advanced Organic Chemistry: Reactions, Mechanisms and Structure* (Smith, M. B., and March, J., eds) pp. 694–695, John Wiley & Sons, Inc., New York
10. Michalak, K., Stepanenko, W., and Wicha, J. (2000) *J. Chem. Soc. Perkin Trans. I* 1587–1594
11. Takeda, K., Osaka, H., Akio, H., Shionogi, *et al.* (1961) *Yakugaku Zasshi* **81,** 325–330
12. Charbonneau, A., and Luu-The, V. (2001) *Biochim. Biophys. Acta* **1517,** 228–235
13. Drury, J. E., and Penning, T. M. (2007) in *Enzymology and Molecular Biology of Carbonyl Metabolism* (Weiner, H., Maser, E., Lindhal, R., and

Plapp, B., eds) pp. 332–340, Purdue University Press, West Lafayette, IN
14. Russell, D. W., and Setchell, K. D. (1992) *Biochemistry* **31,** 4737–4749
15. Russell, D. W. (2003) *Annu. Rev. Biochem.* **72,** 137–174
16. Penning, T. M., Burczynski, M. E., Jez, J. M., Hung, C.-F., Lin, H.-K., Ma, H., Moore, M., Palackal, N., and Ratnam, K. (2000) *Biochem. J.* **351,** 67–77
17. Deyashiki, Y., Taniguchi, H., Amano, T., Nakayama, T., Hara, A., and Sawada, H. (1992) *Biochem. J.* **282,** 741–746
18. Setchell, K. D., Suchy, F. J., Welsh, M. B., Zimmer-Nechemias, L., Heubi, J., and Balistreri, W. F. (1988) *J. Clin. Investig.* **82,** 2148–2157
19. Clayton, P. T., Mills, K. A., Johnson, A. W., Barabino, A., and Marazzi, M. G. (1996) *Gut* **38,** 623–628
20. Kimura, A., Kondo, K.-H., Okuda, K. I., Higashi, S., Suzuki, M., Kurosawa, T., Tohma, M., Inoue, T., Nishiyori, A., Yoshino, M., Kato, H., and Setoguchi, T. (1998) *Eur. J. Pediatr.* **157,** 386–390
21. Gonzales, E., Cresteil, D., Baussan, C., Dabadie, A., Gerhardt, M.-F., and Jacquemin, E. (2004) *J. Hepatol.* **40,** 716–718
22. Lemonde, H. A., Custard, E. J., Bouquet, J., Duran, M., Overmars, H., Scambler, P. J., and Clayton, P. T. (2003) *Gut* **52,** 1494–1499
23. El-Kabbani, O., Green, N. C., Lin, G., Carson, M., Narayana, S. V., Moore, K. M., Flynn, T. G., and DeLucas, L. J. (1994) *Acta Crystallogr. Sect. D Biol. Crystallogr.* **50,** 859–868
24. Wilson, D. K., Bohren, K. M., Gabbay, K. H., and Quiocho, F. A. (1992) *Science* **257,** 81–84
25. Couture, J.-F., Legrand, P., Cantin, L., Luu-The, V., Labrie, F., and Breton, R. (2003) *J. Mol. Biol.* **331,** 593–604
26. Jin, Y., Stayrook, S. E., Albert, R. H., Palackal, N. T., Penning, T. M., and Lewis, M. (2001) *Biochemistry* **40,** 10161–10168
27. Nahoum, V., Gangloff, A., Legrand, P., Zhu, D. W., Cantin, L., Zhorov, B. S., Luu-The, V., Labrie, F., Breton, R., and Lin, S. X. (2001) *J. Biol. Chem.* **276,** 42091–42098
28. Komoto, J., Yamada, T., Watanabe, K., and Takusagawa, F. (2004) *Biochemistry* **43,** 2188–2198
29. Laskowski, R. A., MacArthur, M. W., Moss, D. S., and Thornton, J. M. (1993) *J. Appl. Crystallogr.* **26,** 283–291
30. Couture, J.-F., Legrand, P., Cantin, L., Labrie, F., Luu-The, V., and Breton, R. (2004) *J. Mol. Biol.* **339,** 89–102
31. Hoog, S. S., Pawlowski, J. E., Alzari, P. M., Penning, T. M., and Lewis, M. (1994) *Proc. Natl. Acad. Sci. U. S. A.* **91,** 2517–2521
32. Bennett, M. J., Schlegel, B. P., Jez, J. M., Penning, T. M., and Lewis, M. (1996) *Biochemistry* **35,** 10702–10711
33. Bennett, M. J., Albert, R. H., Jez, J. M., Ma, H., Penning, T. M., and Lewis, M. (1997) *Structure* (*Camb.*) **5,** 799–812
34. Jez, J. M., and Penning, T. M. (1998) *Biochemistry* **37,** 9695–9703
35. Thorn, A., Egerer-Sieber, C., Jäeger, C. M., Herl, V., Müeller-Uri, F., Kreis, W., and Muller, Y. A. (November 21, 2007) *J. Biol. Chem.* 10.1074/jbc.M706185200
36. Otwinowski, Z., and Minor, M. (1997) *Methods Enzymol.* **276,** 307–326
37. McCoy, A. J., Grosse-kunstleve, R. W., Storni, L. C., and Read, R. J. (2005) *Acta Crystallogr. Sect. D Biol. Crystallogr.* **61,** 458–464
38. Jones, T. A., Zou, J.-Y., Cowan, S. W., and Kjeldgaard, M. (1991) *Acta Crystallogr. Sect. A Found. Crystallogr.* **47,** 110–119
39. Brünger, A. T., Adams, P. D., Clore, G. M., DeLano, W. L., Gros, P., Grosse-Kunstleve, R. W., Jiang, J. S., Kuszewski, J., Nilges, M., Pannu, N. S., Read, R. J., Rice, L. M., Simonson, T., and Warren, G. L. (1998) *Acta Crystallogr. Sect. D Biol. Crystallogr.* **54,** 905–921
40. Sheldrick, G., and Schneider, T. (1997) *Methods Enzymol.* **277,** 319–343
41. Allen, F. H. (2002) *Acta Crystallogr. Sect. D Biol. Crystallogr.* **58,** 380–388
42. Eisenberg, D., Lüthy, R., and Bowie, J. U. (1997) *Methods Enzymol.* **277,** 396–404
43. Krissinel, E., and Henrick, K. (2007) *J. Mol. Biol.* **372,** 774–797
44. Steckelbroeck, S., Jin, Y., Oyesanmi, B., Kloosterboer, H. J., and Penning, T. M. (2004) *Mol. Pharmacol.* **66,** 1702–1711
45. Jin, Y., and Penning, T. M. (2006) *Steroids* **71,** 380–391
46. Gandour, R. (1981) *Bioorg. Chem.* **10,** 169–176
47. Grimshaw, C. E., Bohren, K. M., Lai, C. J., and Gabbay, K. H. (1995) *Biochemistry* **34,** 14374–14384
48. Schlegel, B. P., Jez, J. M., and Penning, T. M. (1998) *Biochemistry* **37,** 3538–3548
49. Coustard, J.-M., Douteau, M.-H., Jacquesy, J.-C., and Jacquesy, R. (1975) *Tetrahedron Lett.* **25,** 2029–2030